TÜBİTAK

Turkish Journal of Earth Sciences

http://journals.tubitak.gov.tr/earth/

Research Article

Turkish J Earth Sci
(2023) 32: 262-274

doi:10.55730/1300-0985.1843

# Variations in coupling and deformation along the Hellenic subduction zone

**Michael FLOYD[1,*], Robert KING[1], Demitris PARADISSIS[2], Hayrullah KARABULUT[3], Semih ERGİNTAV[4], Kostas RAPTAKIS[2], Robert REILINGER[1]**

[1]Department of Earth, Atmospheric and Planetary Sciences, Massachusetts Institute of Technology, Cambridge, USA
[2]Department of Topography, National Technical University of Athens, Athens, Greece
[3]Department of Geophysics, Kandilli Observatory and Earthquake Research Institute, Boğaziçi University, İstanbul, Turkey
[4]Department of Geodesy, Kandilli Observatory and Earthquake Research Institute, Boğaziçi University, İstanbul, Turkey

**Received:** 01.04.2022 • **Accepted/Published Online:** 14.09.2022 • **Final Version:** 28.04.2023

**Abstract:** GNSS observations in and around the Aegean Sea, Peloponnese, and western Turkey are sufficiently precise and densely spaced to provide an image of the deformation associated with the Hellenic subduction zone. To isolate deformation associated with the plate boundary, we use GNSS secular velocities and shallow earthquake locations to determine an upper plate reference frame with low internal deformation (<2 mm/yr) that includes a large area of the central and western Aegean. We interpret upper plate deformation as resulting from stronger coupling on the subduction plate interface beneath western Crete than on the western or eastern segments of the Hellenic subduction zone, and the geometry of the subducting plate along-strike. If the long-term tectonic extension of the Aegean upper plate counteracts some of the contractional deformation signal from elastic strain accumulation on the subduction interface, as measured at the surface, the coupling coefficient may be as high as 40% around western Crete, although this is the upper limit.

**Key words:** GNSS, tectonics, Hellenic subduction zone, Aegean

## 1. Introduction and tectonic setting

Building on a long history of geologic investigations (Şengör and Yilmaz, 1981, and references therein), more recent instrumental earthquake records, physical oceanographic studies and satellite imagery, McKenzie (1970, 1972) and Le Pichon and Angelier (1979) used plate tectonic concepts to determine the broad patterns of deformation in the Mediterranean region where the African (Nubian), Arabian and Eurasian plates interact. These studies indicate that two major tectonic processes contribute to the deformation of the Anatolian-Aegean region: collision of Arabia with eastern Anatolia and subduction along the Hellenic subduction zone. Arabia collision builds and supports the topography of the Turkish-Iranian plateau, which induces westward lateral motion of Anatolia, facilitated by the North and East Anatolian Faults (e.g., Şengör and Yilmaz, 1981), while subduction along the Hellenic subduction zone provides a low-resistance plate boundary, which either promotes the Aegean to override the subducting Nubian plate or induces southward motion of the upper plate by a mechanism such as slab rollback (e.g., Le Pichon and Angelier, 1979; Royden, 1993). While discussions of the roles of these two processes continue, there is little debate that a source of deviatoric stress along the Hellenic subduction zone is required to explain the trenchward velocities observed in the Aegean relative to Nubia, the subducting plate (e.g., England et al., 2016).

Many important studies have refined understanding of plate interactions in the Anatolian-Aegean region; we refer the reader to the recent review by Royden and Faccenna (2018). The Aegean region as a whole has a high rate of seismicity, which is divided into three main areas: shallow seismicity on the interface between the subducting (Nubian) plate and overriding Aegean; shallow seismicity within the upper (Aegean) lithosphere; and deep seismicity associated with deformation of the subducting slab in the mantle lithosphere down to depths of approximately 150 km (see Figure 1). In the first regional geodetic study, Smith et al. (1994) used Satellite Laser Ranging (SLR) to identify directly the rapid motion of the Aegean towards the southwest with respect to Europe and North Africa. McClusky et al. (2000) improved on this early result using more densely spaced and more precise site motions derived from Global Navigation Satellite Systems (GNSS) observations, specifically the Global Positioning System (GPS). The proliferation of government, commercial and geophysical GNSS networks, and the recognition that international cooperation is essential to operate global

* Correspondence: mfloyd@mit.edu

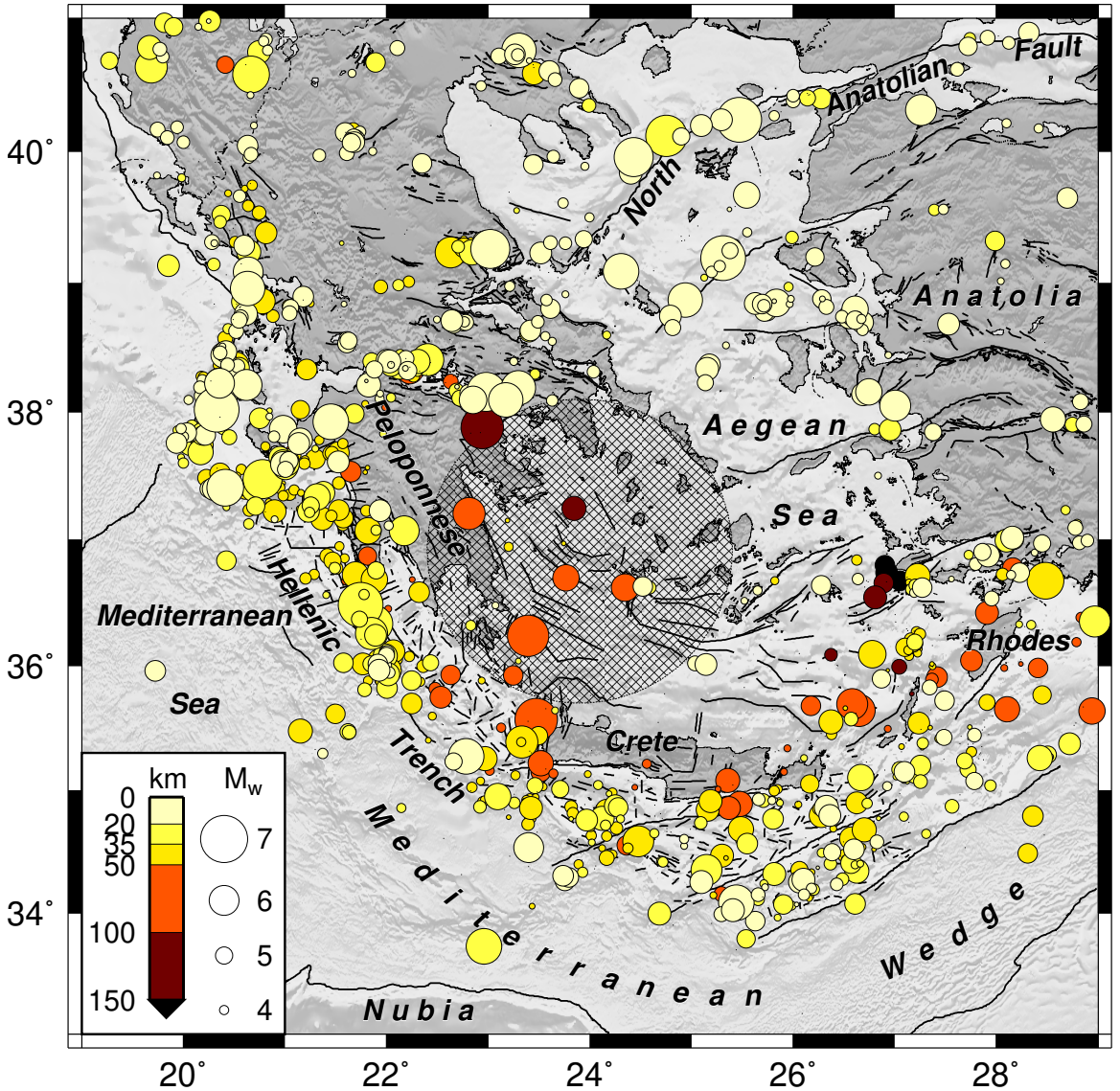


**Figure 1.** Tectonic setting and seismicity of the southern Aegean region. Earthquakes from the ISC-EHB catalog (http://www.isc.ac.uk/isc-ehb/) are plotted according to depth and magnitude, showing the lack of shallow crustal seismicity (yellow dots) in the eastern Peloponnese and western central Aegean (cross-hatched circle), which corresponds to the region of minimal geodetically-observed deformation. Shaded relief topography is from SRTM30 (Farr et al., 2007), and bathymetry from GEBCO (Weatherall et al., 2015).

networks (e.g., Dow et al., 2009), have resulted in a wealth of data that has fostered many subsequent studies. In this study, we report recent GNSS results for the Aegean region, with a focus on the active deformation of the Hellenic subduction zone and its relationship to coupling on the plate interface and processes within the subducting Nubian plate.

## 2. GNSS velocity field

We present the latest version of our geodetic (GNSS; specifically, GPS) velocity solution for the Aegean region. Other parts of the velocity solution are presented in Ergintav et al. (2022) for Anatolia. Both sets of the presented GNSS velocities are regional parts of a larger solution. We describe here the basic processing and characteristics of that velocity solution, although the data beyond the extents of the regions described in these papers will not be discussed further here, before focusing on the Aegean region for the remainder of this paper.

We processed survey (episodic) and continuous GNSS observations gained from several publicly available sources (see Acknowledgements) using the GAMIT/

GLOBK software (Herring et al., 2018) following standard procedures (e.g., Reilinger et al., 2006; McCaffrey et al., 2007). The entire solution, stretching from the Atlas Mountains in the west to the Caucasus Mountains in the east, and from the southern end of the East African Rift in the south to the Eurasian plate in the north, contains data from over 25 years from the start of 1994 to the end of 2018. Only sites whose time series are greater than 2.4 years are included in the solution presented, and survey sites must have a minimum of two occupations that create 2.4-year time series without discontinuities due to earthquakes. The 2.4-year period is chosen to minimize any velocity bias introduced by seasonal variations, which first reaches an acceptable level for time series of that approximate length (e.g., Blewitt and Lavallée, 2002, 2003). Only a small fraction of sites presented here (3.2% of survey sites and 7.9% of continuous sites) have time series shorter than 3 years. The median length of time series is 5.2 years for survey sites and 6.1 years for continuous sites, while the longest time series are over 21 years for survey sites and over 14 years for continuous sites.

We generate and inspect time series for each site to identify discontinuities that are not otherwise defined by the IGS Reference Frame Working Group (e.g., ftp://igs-rf.ign.fr/pub/discontinuities/soln_IGS14.snx) as well as earthquakes likely to have displaced sites in our solution during their observation period. Once we have verified all site perturbations, we fit the continuous daily time series, while accounting for the discontinuities, assuming the presence of temporally correlated noise. We use *Hector* (Bos et al., 2013) to estimate fits to the time series with a white-plus-flicker noise model by maximum likelihood estimation; the fits include linear rate, seasonal (annual plus semiannual) terms and any discontinuities identified, as described above. The velocity uncertainties estimated by *Hector* for each component at each site are converted to equivalent random walk noise magnitudes based on the length of each site's time series using the Equation (2) of Zhang et al. (1997). The median equivalent random walk process noise across all continuous sites is (e, n, u) = (5.18, 5.21, 23.30) $\times$ $10^{-7}$ $mm^2$/yr. The survey and continuous GNSS time series are consolidated into monthly combinations and the velocity solution is finally generated using these monthly solutions, and their associated full covariance matrix, through GLOBK's Kalman filter, with the median equivalent random walk process noise applied to all survey sites, which cannot have their temporally correlated noise assessed directly, as the continuous sites can. The velocity solution is ultimately expressed in of the International Terrestrial Reference Frame (ITRF2014; Altamimi et al., 2016) by minimizing the misfit between observed and model velocities at many sites. The weighted root-mean-square misfit is (e, n, u) = (0.17, 0.14, 0.38) mm/yr. Finally, we exclude any sites whose formal (1-sigma) velocity uncertainty in either horizontal component is greater than 1.5 mm/yr, a fairly conservative value for such a sigma limit.

Figure 2 shows survey and continuous GNSS velocities with respect to Nubia (defined by Altamimi et al., 2017) in the Aegean region that we use in this study. Table S1 also lists these velocities relative to Nubia (shown in Figure 1), our Aegean reference frame (shown in Figure 3; see Section 2.1, below) and Eurasia (shown in Figure S1). Within the region shown in Figure 2 (and Figure S1), we present 221 survey sites and 133 continuous sites.

## 3. Kinematic analysis

### 3.1. Defining a central Aegean reference frame

As indicated in Figure 2, GNSS sites in the Aegean south of the Gulf of Corinth (around 35.5°N) are moving rapidly and roughly coherently towards Nubia, which subducts below the Aegean at the plate boundary, at approximately 34 mm/yr and, correspondingly, away from stable Eurasia at approximately 30 mm/yr because of the small northward motion of Nubia with respect to Eurasia (McClusky et al., 2000; Figure S1). These regional motions, commonly presented relative to either Eurasia or Nubia, obscure more subtle variations within the upper plate itself and possible deformation associated with the subduction zone. Estimating detailed strain rates directly is severely limited by the large distances between islands and uneven distribution of GNSS sites above the subduction zone. Accordingly, to reveal clearly deformation of the upper plate, we define a local Aegean reference frame, with relatively low deformation rates, and plot velocities with respect to it (Figure 3). The low level of shallow seismic activity in the central Aegean (cross-hatched circle in Figure 1) facilitates this approach and guides our choices of sites. It is important to note that strain rates are unchanged by rotating the velocity field into any reference frame.

We selected a set of sites to define a central Aegean reference frame, guided by seismicity, by first using all GNSS velocities in the eastern Peloponnese and Cyclades Islands, then estimating a rotation rate vector to minimize the residual velocities to this fit and iteratively excluding the site whose residual velocities is largest relative to its associated uncertainties (at 95% confidence) before estimating the rotation rate vector again until no sites have a statistically significant residual velocity outside the associated confidence ellipse. One realization of the velocity field, which illustrates well the internal deformation of the Aegean, is shown in Figure 3 (another realization is shown in Figure S2). The residual deformation among the sites used to define the Aegean reference frame is less than 2 mm/yr.

Distinct features of the velocity field across the upper plate, which now become apparent, include an abrupt

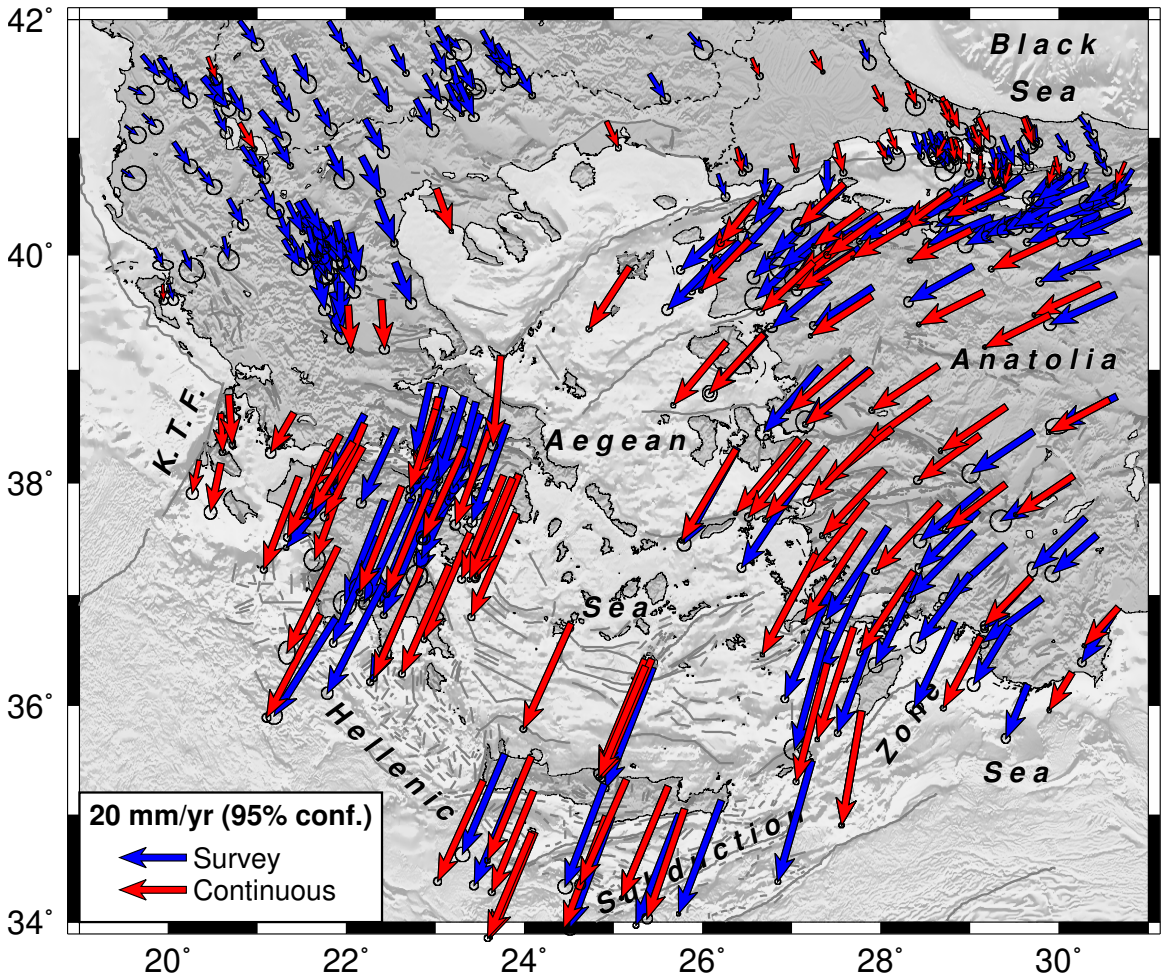


**Figure 2.** Velocities from the GNSS solution relative to Nubia. Within the region shown in this figure are 221 survey sites (blue) and 133 continuous sites (red) with horizontal velocity uncertainties of less than 1.5 mm/yr. Extension between Eurasia (at the northern edge of the figure) and the Aegean near the convergent plate boundary at the Hellenic subduction zone is seen by the increasing magnitude of velocity from northern Greece to the southern Peloponnese, Crete, and Rhodes.

change in central Crete between a small but significant contraction of the upper plate around western Crete and extension around eastern Crete, as also noted previously by Saltogianni et al. (2020) and Briole et al. (2021); higher rates of trench-ward motion of the eastern upper plate compared to the western upper plate (both end of the subduction zone show trench-ward motion and extension in the upper plate, most pronounced at the eastern end, but also occurring at a lower rate along the western-central Peloponnese); and along-strike extension of the upper plate as it overrides the subducting Nubian Plate (Le Pichon and Angelier, 1979; Floyd et al., 2010). Extension both perpendicular and parallel to the strike of the Hellenic subduction zone is observed, showing a broad horizontal extension rate of the southern part of the Aegean upper plate.

### 3.2. Strain accumulation along the Hellenic subduction zone near Crete

The 365 AD, M~8.5 Crete tsunami-generating earthquake was the largest earthquake in the Mediterranean in historic time (Shaw et al., 2008). The earthquake produced uplifted shorelines around the western part of Crete reaching 10 m above sea level, diminishing eastward and reaching only as far as central Crete. No uplifted shorelines were recorded on Gavdos Island, located ~45 km offshore of western Crete (Figure 3). No comparable event has struck the subduction zone in more than 1650 years since then. This long hiatus and the rapid rate of convergence across the subduction zone (~35 mm/yr) require substantial creep on the plate interface (e.g., Jackson and McKenzie, 1988), a view confirmed, although poorly constrained, by analysis of

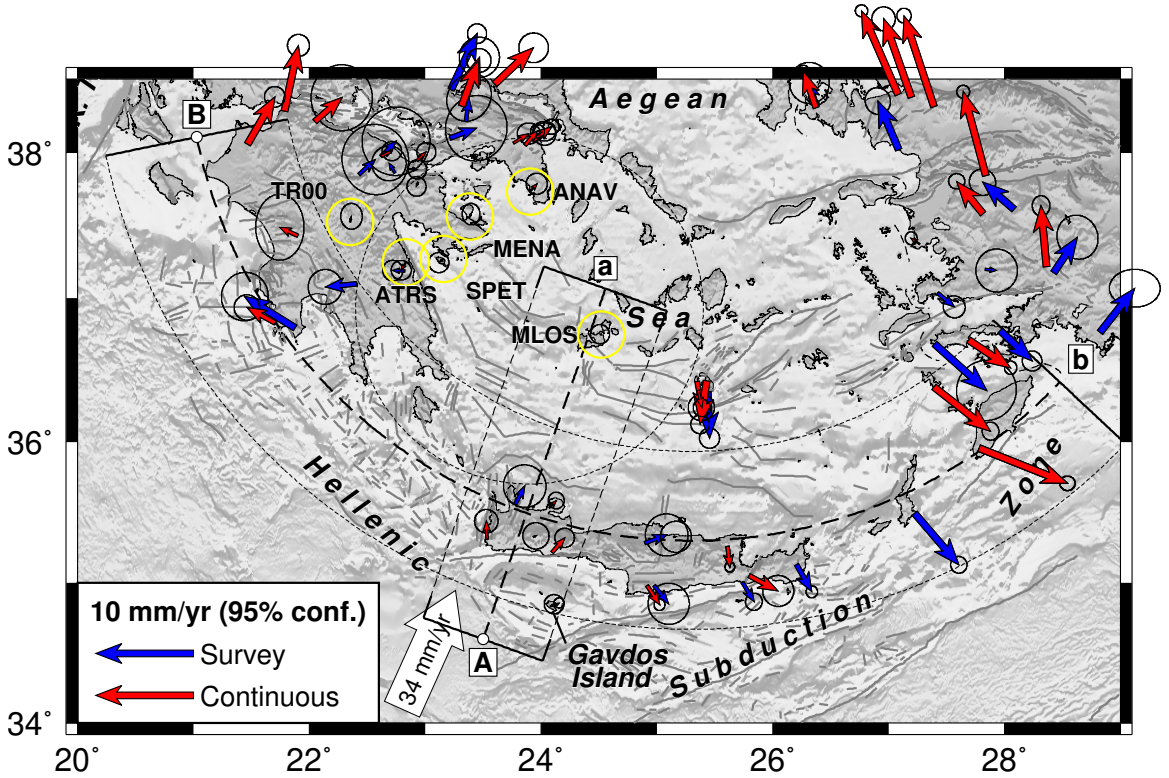


**Figure 3.** Velocities from the GNSS solution in an Aegean (upper plate) reference frame, determined by minimizing the velocities of reference sites circled in yellow and annotated. The large circle around the reference sites corresponds to the cross-hatched area in Figure 1. Velocity profiles A and B are shown in Figure 4. Within the region shown in this figure are 34 survey sites (blue) and 53 continuous sites (red) with horizontal velocity uncertainties of less than 1.5 mm/yr.

geodetic strain rates across the upper plate (Floyd et al., 2010, Vernant et al., 2014).

The long time since the earthquake rules out postseismic effects influencing the present-day velocities. We therefore consider observable deformation as resulting from the strain accumulation cycle that gave rise to the earthquake. Figure 4 shows a simple elastic model for strain accumulation on the Hellenic subduction interface between the subducting Nubian slab and the overriding Aegean. We consider the subduction interface to be a plane dipping at 15°–20° and outcropping at approximately the location of the bathymetric trough on the northern edge of the Mediterranean Wedge, which approximates the plane through shallow thrust seismicity below and offshore of southwest Crete, and crustal depths from receiver function analysis (e.g., Li et al., 2003; Floyd, 2009). This is similar to the subduction interface used by Shaw et al. (2008). We invert for slip deficit rate on the fault, given a fixed locking depth, using a uniform backslip model (e.g., Savage, 1983) with only the horizontal (profile-parallel) component of velocity (shown in the top panel of Figure 4A) because GNSS vertical velocities are less precise and possibly inaccurate, particularly without good control on antenna heights for survey measurements. In any case, tests show that including the vertical component produces only negligible differences in the estimates of slip deficit rate within the formal uncertainty.

We consider a range of potential locking depths from 30 km to 40 km (the shallow thrust seismicity associated with the subduction interface cuts off at a depth of about 40 km below Crete). The estimated slip rate deficit on the subduction interface ranges from 3.3 mm/yr to 6.9 mm/yr given within these bounds on the shallow megathrust geometry, equivalent to a coupling coefficient of about 10%–20% of the plate convergence rate across the subduction zone boundary. The corresponding range of models for these dips (15° and 20°) and locking depths (30 km and 40 km) are shown in the top (profile-parallel) and bottom (vertical) panels of Figure 4A. The various models, unfortunately, lack constraints to the south of Crete, where small differences between them start to become apparent. Furthermore, none of the models are satisfactorily able to fit the horizontal velocities on the island of Gavdos (left two points, near 40 km along the profile, in Figure 4A), which are excluded from the final inversion, and some of the models also do not fit the vertical velocities on Gavdos. This is discussed more in Section 4.2, below.

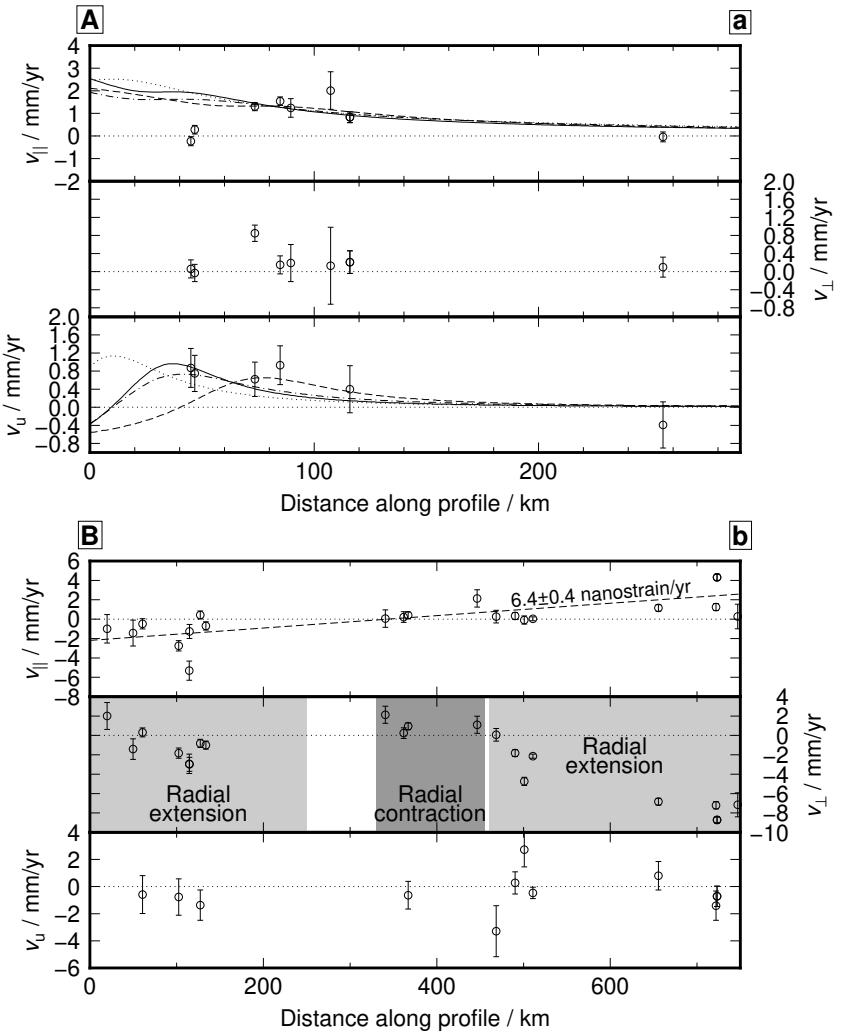


**Figure 4.** Profiles A and B through the velocity solution shown in Figure 3. For both profiles, the top panel is velocity parallel to the profile, i.e. approximately parallel to the dip of the subduction zone for Profile A and parallel to the strike of the subduction zone for Profile B; the middle panel is the velocity perpendicular to the profile, i.e. approximately perpendicular to the dip of the subduction zone for Profile A and perpendicular to the strike of the subduction zone for Profile B; the bottom panel shows vertical velocities. Backslip models shown for Profile A are: dip 15°, locking depth 30 km, estimated slip deficit rate 4.8 ± 0.4 mm/yr (solid line); dip 15°, locking depth 40 km, estimated slip deficit rate 3.3 ± 0.3 mm/yr (dashed line); dip 20°, locking depth 30 km, estimated slip deficit rate 6.9 ± 0.6 mm/yr (dotted line); and dip 20°, locking depth 40 km, estimated slip deficit rate 4.4 ± 0.4 mm/yr (dash-dotted line).

### 3.3. Implications of upper plate deformation

When we define any reference frame, the implicit geodetic goal is to define a set of sites that move coherently relative to one another within their velocity uncertainties. We expect random residuals relative to such a plate reference frame for a well-behaved rigid plate but we do not expect to see systematic patterns of residuals, as this would indicate a deformation in addition to a coherent plate rotation rate. Our approach to selecting sites to define an Aegean upper plate reference frame ultimately does not include sites in western Crete due to their statistically significant motion relative to sites further from the subduction interface. This is in contrast to other authors (e.g., Reilinger et al., 2006; Briole et al., 2021) whose central Aegean blocks often include western Crete, which tends to mask the signature of contraction between western Crete and the central Aegean. Relative to our definition of the upper plate, systematic extension is seen almost everywhere within the rest of the Aegean, even to some extent, within uncertainty, among the sites defining the reference frame. Figures 3 (velocities) and 4 (profiles) show this systematic extension in large parts of the southern Aegean, and is seen on baselines perpendicular to the trend of the Hellenic subduction zone, such as between ANAV and ATRS (see

Figures 3 and S2), which are separated by 110 km and observed to move apart from one another at a rate of 2.0 mm/yr (approximately 18 nanostrain/yr).

We extend this observation to calculate the expected trenchward velocities at the plate boundary, relative to the defined reference frame, given the simple assumption of a deforming upper plate with a homogeneous horizontal strain rate, rather than an otherwise rigid upper plate, as is the case in most studies of upper plate deformation due to subduction. The along-profile (tangential to the strike of the subduction zone) velocities in the top panel of Figure 4B show an extension along the trend of the subduction zone. We assume this velocity gradient is constant and fit the velocities with a straight line by least-squares. Assuming linear extension along the trend of Profile B, we estimate an equivalent strain rate of 6.4 nanostrain/yr or approximately 5 mm/yr over the 750 km length of Profile B (Figure 4B). If we consider the entire southern Aegean above the Hellenic subduction zone to be uniformly straining in the horizontal plane at this (lower) rate, and we consider a central point about which the plate boundary interface circumscribes a small circle to be at approximately 25.3°E 38.7°N, we would predict a trenchward radial velocity of about 2.5 mm/yr at the distance of the southwestern coast of the Peloponnese (~380 km away), the southern coast of Crete (~400 km away) and the southeastern coast of Rhodes (~375 km away). This is not enough to explain the observed radial velocities, particularly around Rhodes where the radial velocity relative to the central Aegean is 6 mm/yr or greater (TILO is 7.3 mm/yr and KATC is 9.7 mm/yr).

Furthermore, if we consider the expected radial velocity, given this uniformly straining upper plate, around southwest Crete to be 2.5 mm/yr, we require at least 4.5 mm/yr of contraction due to locking on the subduction interface to explain the observations seen around southwest Crete in Figure 3 and modeled in Figure 4A. So the slip rate deficit on the subduction interface beneath southwest Crete might be about twice as much as we model using the raw observations alone. However, assuming a uniformly straining upper plate, we still predict no more than 40% of the plate convergence rate to be accumulating as a slip deficit on the Hellenic subduction zone.

## 4. Discussion

The distinct, and well-defined change to slower trenchward motions in central Crete would appear to require a similarly distinct change in the causal process(es). The right-lateral motion indicated by the GNSS observations corresponds to the right-lateral offset in the southern Crete coastline, although there is no comparable offset on the north coast (Figure 3). However, active tectonic studies of Middle-Late Quaternary faulting in Crete (Caputo et al., 2010) indicate only northeast-southwest-striking, southeast-dipping, and relatively minor normal faulting in this region. Strain accumulation on a right-lateral crustal fault is unsupported and seems unlikely.

Two differences between the eastern and western sides of Crete that might provide a physical mechanism for the observed velocity gradient across central Crete include the presence of the Gavdos sea mount offshore of southwestern Crete and the 365 AD earthquake that struck off southwestern Crete.

### 4.1. Independent motion of the Gavdos block

The two GNSS velocities from the island of Gavdos (the two points furthest to the left, around 40 km along the profile, in Figure 4A) are anomalous to fit with any realistic model of elastic strain accumulation on the subduction zone beneath western Crete. Their near zero horizontal velocity relative to the Aegean reference frame (e.g., Milos in the volcanic arc) combined with their clear uplift does not conform to the models of elastic strain accumulation on the Hellenic subduction interface proposed here. There are deep trench systems, most likely as a result of large upper crustal, or even through-crustal, faults between Gavdos and the south coast of Crete to the north and the Hellenic Trench to the south. We hypothesize that the island of Gavdos is situated on a relatively independent block which is decoupled and isolated from the motion of both the subducting Nubian slab and the overriding crust of the central Aegean, caught between them and acting largely independently as a result. Mapped faults between western Crete and Gavdos (e.g., NOAFAULTs v4.0; Ganas, 2022) are west- and WNW-striking faults dipping steeply (~60°) to the north, and mapped faults to the south of Gavdos Island are east and ESE-striking, dipping steeply to the south. These features suggest that Gavdos may sit atop the footwall of normal faults in the upper plate, above the main subduction interface within the broad convergent region at depth. This has also been incorporated as a correction to GNSS velocities by Saltogianni et al. (2020) before their modeling of the subduction interface.

### 4.2. Deformation along the eastern and western ends of the subduction zone

On the basis of regional tectonics and early seismic tomography (Wortel and Spakman, 1992), Barka and Reilinger (1997) suggested that the high rates of motion where the eastern Aegean overrides the subducting Nubian oceanic plate may be related to a tear in the subducting slab. In support of this interpretation, Figures 5 and 6 show rapid variations in the depth of intermediate seismicity along the eastern end of the subduction zone near Rhodes, and Figure 7 shows a horizontal slice through a seismic tomography image of the Aegean and western Anatolia (Karabulut et al. 2019; Aksari, 2019) at a depth of 100 km.

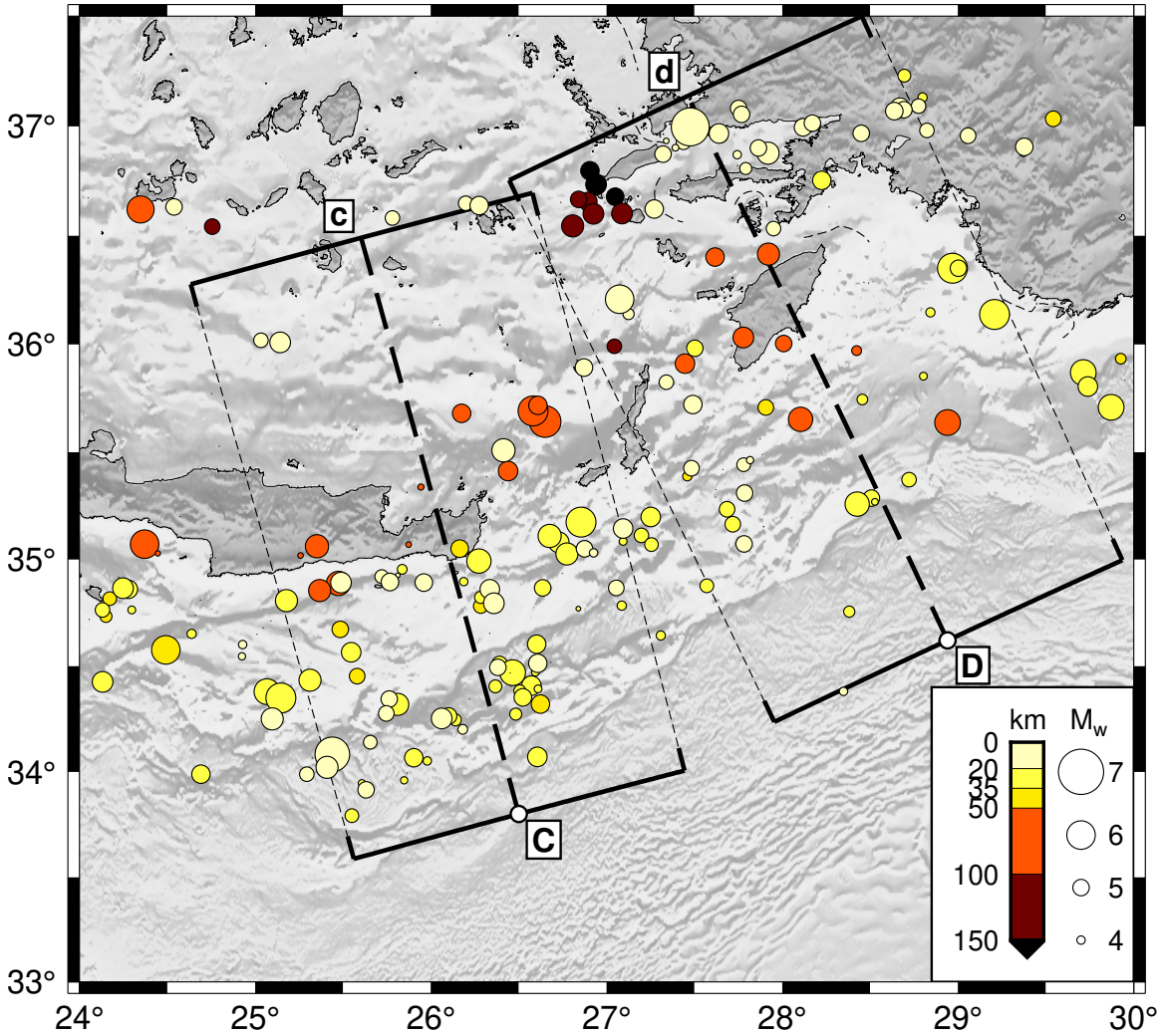


**Figure 5.** ISC-EHB seismicity, as in Figure 1, where only events with good depth control are plotted (Levels 1 and 2, as defined under "Searching the ISC-EHB database" at http://www.isc.ac.uk/isc-ehb/). Profiles are chosen to be approximately parallel to the dip of the subduction zone and shown in cross-section in Figure 6 with the corresponding seismic tomography.

Fast velocities, represented by blue, indicate that the subducted slab beneath the Aegean and western Anatolia are disconnected. Depth cross-sections in Figure 6 further reveal a continuous slab beneath the central Aegean as reported earlier by Wortel and Spakman (2000) and, additionally, an apparent discontinuity in the slab below 100 km beneath the eastern end of the Hellenic subduction zone and southwest Anatolia. According to this hypothesis, the slab tear detaches the Hellenic slab from the more shallow-dipping Cyprus slab beneath the eastern end of the Hellenic subduction zone. This allows the eastern side of Hellenic slab to sink, inducing southwest extension of the overriding plate. Such rapid trenchward motion does not preclude strain accumulation along the subduction interface; indeed, uplifted shorelines in Rhodes have been interpreted to be due to an ancient, tsunami-generating earthquake 3500–4000 B.P. (England et al., 2015, and references therein), as with the 365 AD event, with the long hiatus being consistent with creep dominating convergence.

Trenchward extension, although considerably smaller, is also apparent in the western Peloponnese along the western end of the Hellenic subduction zone (Figure 3). Deformation at this end of the subduction zone is complex, involving the interaction of rapid extension across the Gulf of Corinth (e.g., Armijo et al., 1996), right lateral strike-slip on the Kephalonia transform fault (e.g., Karitza and Louvari, 2003), and the junction between continental subduction and collision north of the Kephalonia transform fault with ocean subduction to the south (Pearce et al., 2012). The rate of extension with respect to

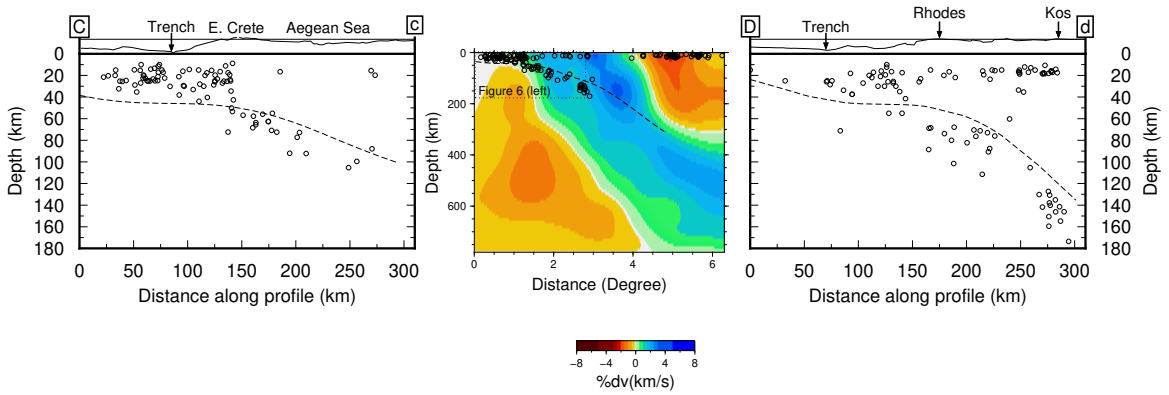


**Figure 6.** (Left and Right) Profiles through ISC-EHB seismicity along the two profiles (C and D) shown in Figure 5. The top sections show topographic profiles and the bottom sections show cross-sections through the ISC-EHB catalog (Levels 1 and 2 only, as defined under "Searching the ISC-EHB database" at http://www.isc.ac.uk/isc-ehb/). The dashed lines are the projected slab geometry from Slab2 (Hayes et al., 2018). (Center) Profile through the ISC-EHB catalog and seismic tomography described in Section 3.4 along approximately the same line as Profile C.

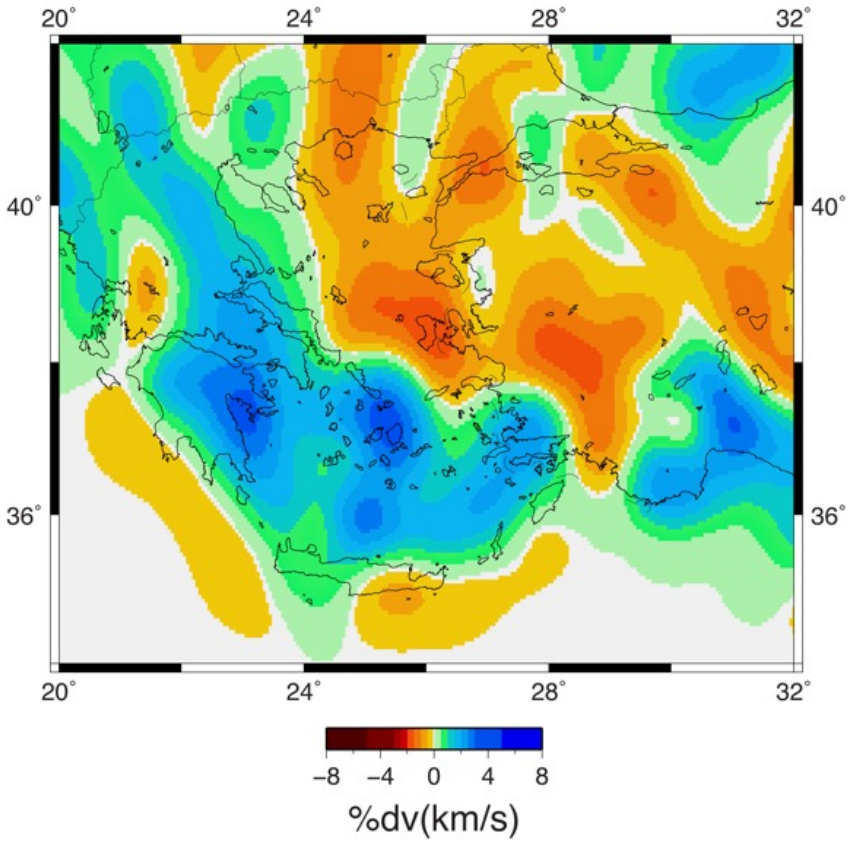


**Figure 7.** Slice through the seismic tomography discussed in Section 4.2, relative to a reference velocity of 8.1 km/s at 100 km depth. The details of tomography are given in Karabulut et al. (2019) and Aksarı (2019).

the central Aegean, 3–4 mm/yr, is less than half that across the eastern Aegean (~10 mm/yr). Whether there is a break and offset, or a down-warping of the oceanic slab beneath the northern Peloponnese relative to the continental subducting slab north of the transform, is still unclear (Suckale et al., 2009; Pearce et al., 2012). However, either a slab tear or active down-warping could induce trenchward extension of the upper plate.

In addition to east-west extension, the westernmost Peloponnese have a well-defined, along-strike component of north- and northwest-directed motion relative to the central Aegean, and indeed relative to Crete and the southeastern Aegean (Figures 3, S2). These small motions (~2-3 mm/yr relative to the central Aegean) result in along-strike extension that has been interpreted to result from the flow of the Aegean lithosphere over the subducting slab (e.g., Le Pichon and Angelier, 1979).

We interpret these variations of the slab depth and geometry as influencing the pattern of deformation observed at the surface. Underneath western Crete, the slab appears to be shallower and less steeply dipping with a colder (Pn tomography) contact with the upper crust at the Moho (Figure 8; Mutlu and Karabulut, 2011; Karabulut and Ozdeger, 2018). This changes rapidly beneath eastern Crete, where the slab is deeper and/or warmer, potentially allowing reduced friction at the interface to lower coupling between the plates. This may be due to a physical warp or rise in the slab's upper surface geometry below eastern Crete, or a thermal effect due to the influence of a subcrustal wedge of mantle material, which is more prevalent to the west and east of western Crete. Even further east, beneath Rhodes, a more discrete step in the nature of the slab below the crust is observed, compatible with a tear beneath (e.g., Barka and Reilinger, 1997).

Whatever the inducing source of the extension and its variation along the plate boundary, it is clear that such a source of variable deformation along the subduction zone is necessary. England et al. (2016) use a free model parameter for their boundary conditions for the Hellenic subduction zone, although its physical source is not specified. Here we have attempted to model a velocity condition at the boundary by considering the small

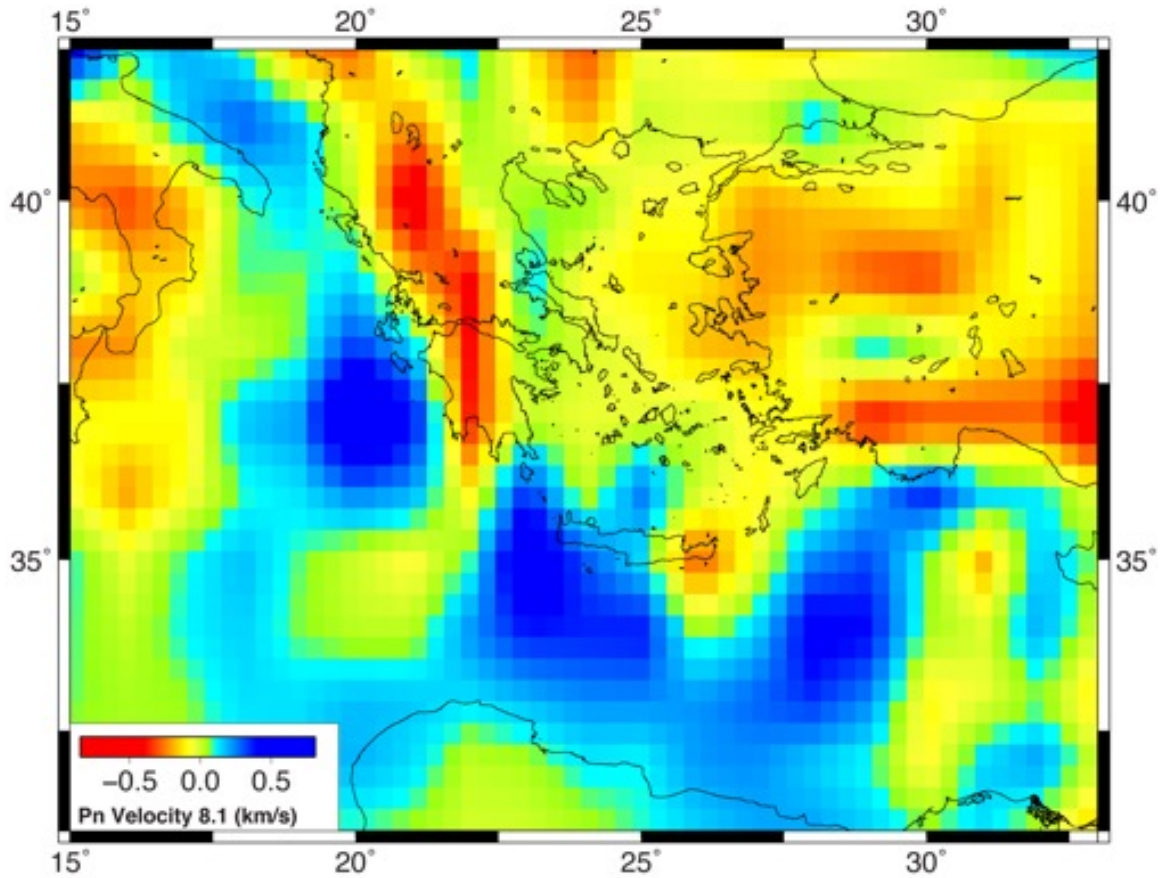


**Figure 8.** Pn tomography showing the variations in sub-Moho seismic velocities in the Aegean-Anatolia region (Karabulut and Ozdeger, 2018). Blue colors correspond to faster velocities, interpreted as being due to cold subcrustal material, and red colors correspond to slower velocities relative to a standard velocity of 8.1 km/s. The Pn velocities show an abrupt transition from fast beneath western Crete to slow beneath eastern Crete and the Dodecanese islands. Western Crete is the only area along the Hellenic subduction zone beneath which there appears to be an incursion of faster Pn velocities, matching the only area where contraction in the upper plate is observed. This suggests a subcrustal process may play an important role in determining the deformation along the plate boundary.

but significant deformation of the upper plate. We agree with England et al. (2016) that the percentage of plate convergence accumulating as elastic strain is likely to be 10%-20%, although it may be about twice that if a deforming upper plate is considered using a simple assumption of homogeneous strain rate, but we hypothesize that any GPE forces are comparable to other external boundary forces such as a down-warping slab, which would produce the same positive (tensional) force as a GPE contrast across the boundary itself.

The region where there is contraction, rather than extension, in the upper plate also corresponds to the highest bathymetry along the trenches of the Hellenic system, relative to deeper troughs to the west (off the southwestern coast of the Peloponnese) and east (off the southeastern coast of Rhodes), which may also indicate that the slab geometry has a defining influence on the deformation of the Aegean region. Ganas and Parsons (2009), for example, previously explored the effect of the three-dimensional geometry of the slab, although discrete features such as a tear in the subducting Nubian plate were not included explicitly.

## 5. Summary

Using GNSS secular velocities and shallow earthquake locations, we determine a local upper plate reference frame in the central Aegean with low internal deformation in order to delineate deformation associated with the Hellenic subduction zone. Our results show a significant difference between the eastern and western segments of the plate boundary, with a distinct change in central Crete. In western Crete, the motion of GNSS sites relative to the Aegean is actually a contraction of the upper plate, suggesting that active strain accumulation is occurring and may be released in a future earthquake, such as the 365 A.D. event. In eastern Crete, the motion of GNSS sites relative to the Aegean reverses to extension, as across most of the region. While the entire upper plate is rapidly converging with Nubia across the trench (~35 mm/yr), the western side from central Crete to the southern part of the Peloponnese has slower trenchward motion than the eastern side. The westernmost Peloponnese deviates from this pattern, displaying an additional small (~2–4 mm/yr), but distinct trenchward motion compared to the remainder of the western Aegean. In contrast, the eastern side, beginning in central Crete, moves trenchward with respect to the central Aegean with rates increasing from ~4 to 10 mm/yr from central Crete to Rhodes near the eastern end of the Hellenic subduction zone. We suggest that the differential motion between the eastern and western segments is due to stronger coupling between the subducting Nubian and over riding Aegean plate along the western plate boundary, either on the subduction interface or a splay fault.

The abrupt change in coupling in central Crete may be related to the collision of the Gavdos Island block with the trench off shore of western Crete that retards trenchward motion. In contrast, the more rapid trenchward motion along the eastern upper plate may be related to a tear in the subducted Nubian lithosphere that allows rapid sinking of the subducting plate, inducing lower coupling on the plate interface and the observed rapid trenchward motion. The slip rate deficit on the subduction zone is approximately 10%–20% and, even assuming a deforming upper plate, is not greater than 40%.

## Acknowledgements

Data processed for the GNSS velocity solution presented here are available from various different sources, including Biliris et al. (2014), CDDIS (Noll, 2010 and IGS Data Center), NOA (http://geodesy.gein.noa.gr:8000/nginfo/), and UNAVCO; see references, below, for full citations. The solution for the region discussed in this paper is provided as a plain text table in the supporting material.

## Supplementary Data

Supplementary data can be accessed at the following link: https://aperta.ulakbim.gov.tr/record/252406#.ZFziMC9Bxqs

## References

Aksarı D (2019). Determination of upper mantle heterogeneity beneath Aegean-Anatolian region from travel time tomography. PhD, Boğaziçi University, Department of Geophysics, İstanbul, Turkey.

Altamimi Z, Rebischung P, Métivier L, Collilieux X (2016). ITRF2014: A new release of the International Terrestrial Reference Frame modeling nonlinear station motions. Journal of Geophysical Research: Solid Earth 121 (8): 6109–6131. https://doi.org/10.1002/2016JB013098

Altamimi Z, Métivier L, Rebischung P, Rouby H, Collilieux X (2017). ITRF2014 plate motion model. Geophysical Journal International 209 (3): 1906–1912. https://doi.org/10.1093/gji/ggx136

Armijo R, Meyer B, King GCP, Rigo A, Papanastassiou D (1996). Quaternary evolution of the Corinth Rift and its implications for the Late Cenozoic evolution of the Aegean. Geophysical Journal International 126 (1): 11–53. https://doi.org/10.1111/j.1365-246X.1996.tb05264.x

Barka A, Reilinger R (1997). Active tectonics of the Eastern Mediterranean region: deduced from GPS, neotectonic and seismicity data. Annals of Geophysics 40 (3): 587–610. https://doi.org/10.4401/ag-3892

Biliris H, England P, Floyd M, Nocquet J-M, Palamartchouk K et al. (2014). COMET: Continuous GPS measurements from the Aegean from 2002 to present. NERC Earth Observation Data Centre. http://catalogue.ceda.ac.uk/uuid/8aa71e3a6899480baea9d0f7e8e21239

Blewitt G, Lavallée D (2002). Effect of annual signals on geodetic velocity. Journal of Geophysical Research 107 (B7): ETG 9-1–ETG 9-11 https://doi.org/10.1029/2001JB000570

Blewitt G, Lavallée D (2003). Correction to "Effect of annual signals on geodetic velocity". Journal of Geophysical Research 108 (B1): ETG 4-1–ETG 4-1. https://doi.org/10.1029/2002JB002297

Bos, MS, Fernandes RMS, Williams SDP, Bastos L (2013). Fast error analysis of continuous GNSS observations with missing data. Journal of Geodesy 87 (4): 351–360. https://doi.org/10.1007/s00190-012-0605-0

Briole P, Ganas A, Elias P, Dimitrov D (2021). The GPS velocity field of the Aegean. New observations, contribution of the earthquakes, crustal blocks model. Geophysical Journal International 226 (1): 468–492. https://doi.org/10.1093/gji/ggab089

Caputo R, Catalano S, Monaco C, Romagnoli G, Tortorici G et al. (2010). Active faulting on the Island of Crete (Greece). Geophysical Journal International 183 (1): 111–126. https://doi.org/10.1111/j.1365-246X.2010.04749.x

Dow MJ, Neilan RE, Rizos C (2009). The International GNSS Service in a changing landscape of Global Navigation Satellite Systems. Journal of Geodesy 83 (–4): 191–198. https://doi.org/10.1007/s00190-008-0300-3

England P, Howell A, Jackson J, Synolakis C (2015). Paleotsunamis and tsunami hazards in the Eastern Mediterranean. Philosophical Transactions of the Royal Society A 373 (2053): 20140374. https://doi.org/10.1098/rsta.2014.0374

England P, Houseman G, Nocquet J-M (2016). Constraints from GPS measurements on the dynamics of deformation in Anatolia and the Aegean. Journal of Geophysical Research: Solid Earth 121 (12): 8888–8916. https://doi.org/10.1002/2016JB013382

Ergintav S, Floyd M, Paradissis D, Karabulut H, Vernant P et al. (2022). New geodetic constraints on the role of faults and blocks versus distributed strain in the Nubia-Arabia-Eurasia zone of active plate interactions. Turkish Journal of Earth Sciences 31. https://doi.org/10.55730/yer-2205-5.

Farr, TG, Rosen PA, Caro E, Crippen R, Duren R et al. (2007). The Shuttle Radar Topography Mission. Reviews of Geophysics 45 (2): RG2004. https://doi.org/10.1029/2005RG000183

Floyd MA (2009), Continuous and survey Global Positioning System observations of the deformation of the Aegean. DPhil, University of Oxford, U.K.

Floyd M, Billiris H, Paradissis D, Veis G, Avallone A et al. (2010). A new velocity field for Greece: Implications for the kinematics and dynamics of the Aegean. Journal of Geophysical Research 115 (B10): B10403. https://doi.org/10.1029/2009JB007040

Ganas A (2022). NOAFAULTS KMZ layer Version 4.0 (V4.0). Zenodo. https://doi.org/10.5281/zenodo.6326260

Ganas A, Parsons T (2009). Three-dimensional model of Hellenic Arc deformation and origin of the Cretan uplift. Journal of Geophysical Research 114 (B6): B06404. https://doi.org/10.1029/2008JB005599

Hayes G, Moore GL, Portner DE, Hearne M, Flamme H et al. (2018). Slab2, a comprehensive subduction zone geometry model. Science 362 (6410): 58–61. https://doi.org/10.1126/science.aat4723

Herring TA, King RW, Floyd MA, McClusky SC (2018). Introduction to GAMIT/GLOBK, Release 10.7. Cambridge, MA, USA: Massachusetts Institute of Technology.

International GNSS Service. Daily 30-second observation data. Greenbelt, MD, USA: NASA Crustal Dynamics Data Information System (CDDIS). https://doi.org/10.5067/GNSS/gnss_daily_o_001

Jackson J, McKenzie DP (1988). The relationship between plate motions and seismic moment tensors, and the rates of active deformation in the Mediterranean and Middle East. Geophysical Journal International 93 (1): 45–73. https://doi.org/10.1111/j.1365-246X.1988.tb01387.x

Karabulut H, Deger Ozbakir A (2018). Pn tomography of the Eastern Mediterranean Region. In: Geophysical Research Abstracts, EGU General Assembly 2018; Vienna, Austria. Volume 20, EGU2018-8663.

Karabulut H, Aksarı D, Değer Özbakır A, Paul A (2019). A new P-wave tomographic model of the Aegean-Anatolia Domain and its implications for small scale dynamics. In: Geophysical Research Abstracts, EGU General Assembly 2019. Volume 21, EGU2019-10365.

Kiratzi A, Louvari E (2003). Focal mechanisms of shallow earthquakes in the Aegean Sea and the surrounding lands determined by waveform modeling: a new database, Journal of Geodynamics 36 (1–2): 251–274. https://doi.org/10.1016/S0264-3707(03)00050-4

Le Pichon X, Angelier J (1979) The Hellenic arc and trench system: A key to the evolution of the Eastern Mediterranean area. Tectonophysics 60 (1–2): 1–42. https://doi.org/10.1016/0040-1951(79)90131-8

Li X, Bock G, Vafidis A, Kind R, Harjes H-P et al. (2003). Receiver function study of the Hellenic subduction zone: imaging crustal thickness variations and the oceanic Moho of the descending African lithosphere. Geophysical Journal International 155 (2): 733–748. https://doi.org/10.1046/j.1365-246X.2003.02100.x

McCaffrey R, Qamar AI, King RW, Wells R, Khazaradze, G et al. (2007). Fault locking, block rotation and crustal deformation in the Pacific Northwest. Geophysical Journal International 169 (3): 1315–1340. https://doi.org/10.1111/j.1365-246X.2007.03371.x

McClusky S, Balassanian S, Barka A, Demir C, Ergintav S et al. (2000). GPS constraints on plate kinematics and dynamics in the eastern Mediterranean and Caucasus. Journal of Geophysical Research 105 (B3): 5695–5719. https://doi.org/10.1029/1999JB900351

McKenzie, DP (1970). Plate tectonics of the Mediterranean region. Nature 226 (5242): 239–243. https://doi.org/10.1038/226239a0

McKenzie, DP (1972). Active tectonics of the Mediterranean region. Geophysical Journal of the Royal Astronomical Society 30 (2): 109–185. https://doi.org/10.1111/j.1365-246X.1972.tb02351.x

McQuarrie N, Stock JM, Verdel C, Wernicke BP (2003). Cenozoic evolution of the Neotethys and implications for the causes of plate motions. Geophysical Research Letters 30 (20): 2036. https://doi.org/10.1029/2003GL017992

Mutlu AK, Karabulut H (2011). Anisotropic Pn tomography of Turkey and adjacent regions. Geophysical Journal International 187 (3): 1743–1758. https://doi.org/10.1111/j.1365-246X.2011.05235.x

Noll, CE (2010). The Crustal Dynamics Data Information System: A resource to support scientific analysis using space geodesy. Advances in Space Research 45 (12): 1421–1440. https://doi.org/10.1016/j.asr.2010.01.018

Pearce, FD, Rondenay S, Sachpazi M, Charalampakis M, Royden L (2012). Seismic investigation of the transition from continental to oceanic subduction along the western Hellenic subduction zone. Journal of Geophysical Research 117 (B7): B07306. https://doi.org/10.1029/2011JB009023

Reilinger, R, McClusky S, Vernant P, Lawrence S, Ergintav S et al. (2006). GPS constraints on continental deformation in the Africa-Arabia-Eurasia continental collision zone and implications for the dynamics of plate interactions. Journal of Geophysical Research 111 (B5): B05411. https://doi.org/10.1029/2005JB004051

Royden L, Faccenna C (2018). Subduction orogeny and the late Cenozoic evolution of the Mediterranean arcs. Annual Review of Earth and Planetary Sciences 46 (1): 261–289. https://doi.org/10.1146/annurev-earth-060115-012419

Royden LH (1993). The tectonic expression of slab pull at continental convergent boundaries. Tectonics 12 (2): 303–325. https://doi.org/10.1029/92TC02248

Saltogianni V, Mouslopoulou V, Oncken O, Nicol A, Gianniou M et al. (2020). Elastic fault interactions and earthquake rupture along the southern Hellenic subduction plate interface zone in Greece. Geophysical Research Letters 47 (13): e2019GL086604. https://doi.org/10.1029/2019GL086604

Savage JC (1983). A Dislocation Model of Strain Accumulation and Release at a Subduction Zone. Journal of Geophysical Research 88 (B6): 4984–4996. https://doi.org/10.1029/JB088iB06p04984

Şengör AMC, Yilmaz Y (1981). Tethyan evolution of Turkey: A plate tectonic approach, Tectonophysics 75 (3–4): 181–241. https://doi.org/10.1016/0040-1951(81)90275-4

Shaw B, Ambraseys NN, England PC, Floyd MA, Gorman GJ et al. (2008). Eastern Mediterranean tectonics and tsunami hazard inferred from the AD 365 earthquake. Nature Geoscience 1 (4): 268–276. https://doi.org/10.1038/ngeo151

Smith DE, Kolenkiewicz R, Robbins JW, Dunn PJ, Torrence MH (1994). Horizontal crustal motion in the central and eastern Mediterranean inferred from Satellite Laser Ranging measurements. Geophysical Research Letters 21 (18): 1979–1982. https://doi.org/10.1029/94GL01612

Suckale J, Rondenay S, Sachpazi M, Charalampakis M, Hosa A et al. (2009). High resolution seismic imaging of the western Hellenic subduction zone using teleseismic scattered waves. Geophysical Journal International 178 (2): 775–791. https://doi.org/10.1111/j.1365-246X.2009.04170.x

Vernant P, Reilinger R, McClusky S (2014). Geodetic evidence for low coupling on the Hellenic subduction plate interface, Earth and Planetary Science Letters 385: 122–129. https://doi.org/10.1016/j.epsl.2013.10.018

Weatherall P, Marks KM, Jakobsson M, Schmitt T, Tani S et al. (2015). A new digital bathymetric model of the world's oceans. Earth and Space Science 2 (8): 331–345. https://doi.org/10.1002/2015EA000107

Wortel, MJR, Spakman W (1992). Structure and dynamics of subducted lithosphere in the Mediterranean region. Proceedings of the Koninklijke Nederlandse Akademie van Wetenschappen 95 (3): 325–347.

Wortel, MJR, Spakman W (2000). Subduction and slab detachment in the Mediterranean-Carpathian region. Science 290 (5498): 1910–1917. https://doi.org/10.1126/science.290.5498.1910

Zhang J, Bock Y, Johnson H, Fang P, Williams S et al. (1997). Southern California permanent GPS geodetic array: Error analysis of daily position estimates and site velocities. Journal of Geophysical Research 102 (B8): 18035–18055. https://doi.org/10.1029/97JB01380

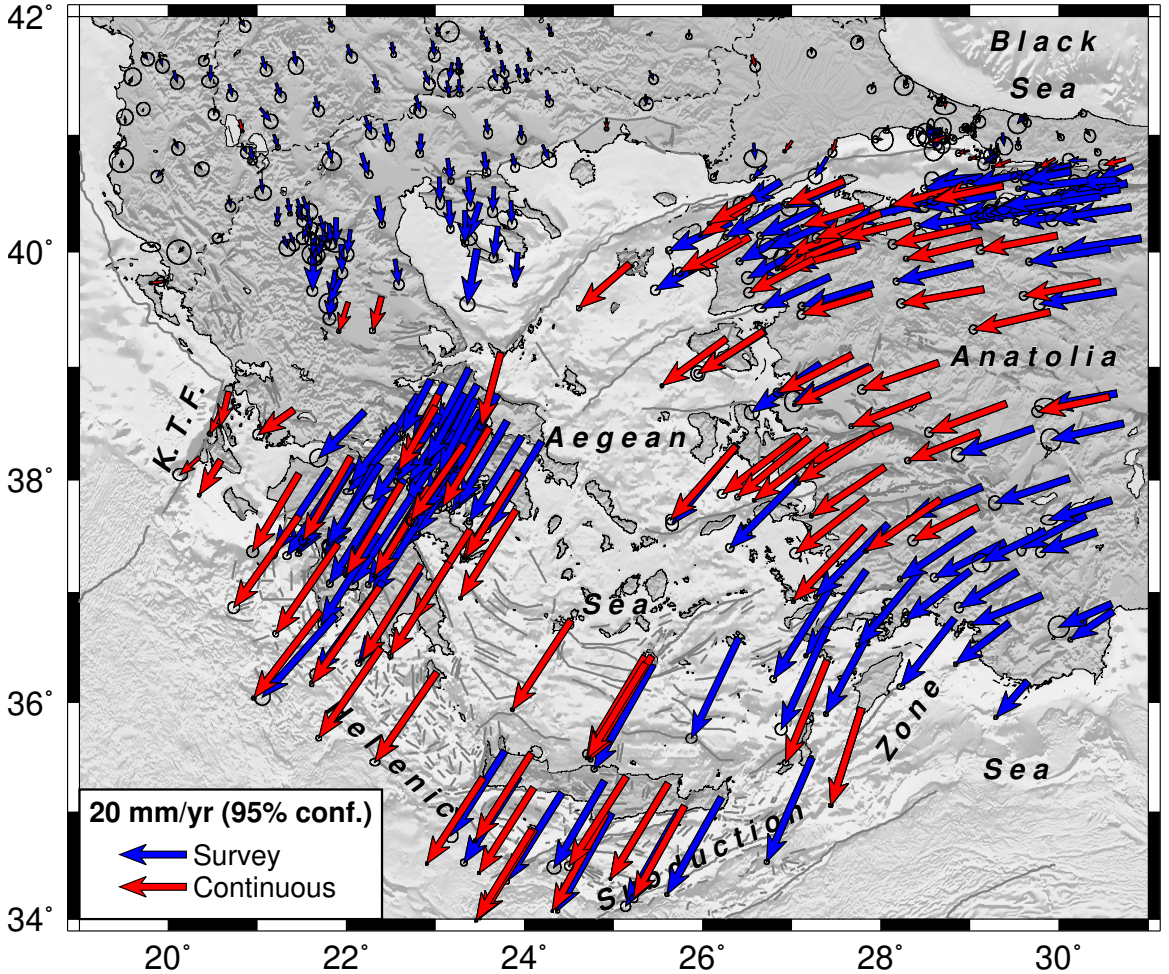


**Figure S1.** Velocities from the GNSS solution, as described in the main text and shown in Figures 1 and 3, relative to Eurasia.

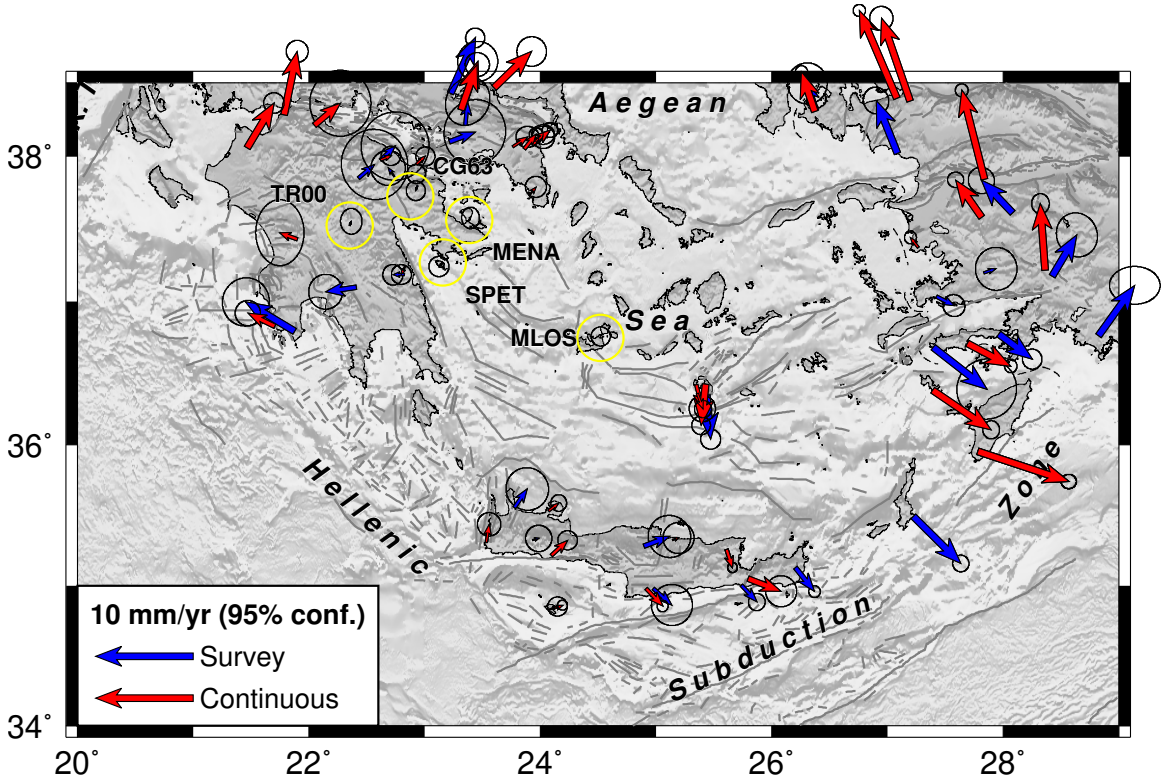


**Figure S2.** An alternative representation of the Aegean (upper plate) reference frame. CG63 is used instead of ANAV and ATRS compared to Figure 2 (see discussion in Section 3.2 of main text). The RMS difference between the two choices of frames for the sites shown is negligible (0.14 mm/yr) compared to the uncertainties of the data (median 0.5 mm/yr). The plate convergence-parallel contraction between southwestern Crete and the central Aegean (e.g., volcanic arc) at a rate of approximately 2 mm/yr, and the velocity gradient between western and eastern Crete, from upper plate contraction to upper plate extension, are seen clearly in both definitions of an Aegean reference frame shown here and in Figure 3.